Colloid Polym Sci 279:800–806 (2001)

ORIGINAL CONTRIBUTION

C. Schick
A. Wurm
A. Mohamed

Vitrification and devitrification of the rigid amorphous fraction of semicrystalline polymers revealed from frequency-dependent heat capacity

Received: 6 December 2000
Accepted: 29 January 2001

C. Schick (✉) · A. Wurm · A. Mohamed
University of Rostock
Department of Physics
18051 Rostock, Germany
e-mail: christoph.schick@physik.uni-rostock.de

Abstract The relaxation strength at the glass transition shows significant deviations from a two-phase model for semicrystalline polymers. The introduction of a rigid amorphous fraction (RAF), which is noncrystalline but does not participate in the glass transition, allows a description of the relaxation behavior. The question arises when does this amorphous material vitrify. Temperature-modulated differential scanning calorimetry measurements allow the online study of heat capacity changes during isothermal crystallization. For bisphenol-A polycarbonate (PC) and poly(3-hydroxybutyrate) (PHB) at reasonably high modulation frequencies (10 mHz), no contribution from reversing melting to the measured heat capacity was detected at the crystallization temperature; therefore, changes in the baseline heat capacity can be studied. The amount of RAF obtained at the crystallization temperature was compared with that obtained from the step in heat capacity at the glass transition at lower temperatures. No changes in the amount of the RAF occur in the temperature range between crystallization and the glass transition. Consequently, the rigid amorphous material is totally established during the isothermal crystallization of PC and PHB. The reason for the vitrification of the RAF is the immobilization of cooperative motions owing to the fixation of parts of the molecules in the crystallites, which is favorable at the fold surfaces. In this way, crystallization in PC and PHB limits itself by vitrifying the crystallizable material next to the growing crystals. On heating, devitrification of the RAF occurs when the crystals, which were formed last, melt in the temperature range of the lowest endotherm.

Key words Glass transition · Temperature-modulated differential scanning calorimetry · Rigid amorphous; Polymers; PC; PHB

Introduction

From the glass transition, it is well known and generally accepted to describe heat capacity by complex numbers. A typical frequency dependence as for other relaxation processes is observed – a sigmoid step in the real and a peak in the imaginary part of the heat capacity [1–3]. Recent measurements also indicate a frequency dependence of the heat capacity of semicrystalline polymers outside the glass-transition range [4, 5]. These observations are related to the occurrence of an excess heat capacity that can be observed in a rather wide temperature range between the glass transition and the melting temperature[1]. The origin of this excess heat capacity and

[1] The term "excess heat capacity, $C_{p,\mathrm{excess}}$" is used here as the difference between the modulus of measured complex heat capcaity and the baseline heat capacity.

its frequency dependence are not yet understood. Probably the molecular processes involved are related to the surface of the polymer crystallites and often the term reversing melting [6] is used. For polymers showing a sliding diffusion in the crystallites (α relaxation in case of polyethylene), large contributions to reversing melting are due to surface melting [7]. For other semicrystalline polymers we do not know which surfaces, growth or fold, are responsible for the process of reversing melting and the corresponding excess heat capacity.

In order to obtain information about the characteristic time scale of the molecular processes related to the excess heat capacity we have studied the frequency dependence of the modulus of complex heat capacity during quasiisothermal crystallization. To extend the frequency range available with temperature-modulated differential scanning calorimetry (TMDSC, 10^{-5}–10^{-1} Hz) alternating current calorimetric measurements were performed at a frequency of 1 Hz [8]. Unfortunately, we are not able to determine the corresponding phase with the necessary precision because of heat transfer problems; therefore, the real and imaginary parts of the complex heat capacity cannot be obtained. The excess heat capacity for polycaprolactone (PCL) is shown in Fig. 1. A mean relaxation time of the order of seconds can be estimated for the process at 328 K. The frequency range available is still not broad enough for a detailed discussion of the curve shape (Fig. 1); however, from the curve one expects to measure a baseline heat capacity without contributions due to reversing melting for frequencies higher than about 100 Hz. The baseline heat capacity corresponds to the heat necessary to increase the temperature of the sample without changing the crystallinity. In other words, it is the heat capacity without any contribution from latent heats.

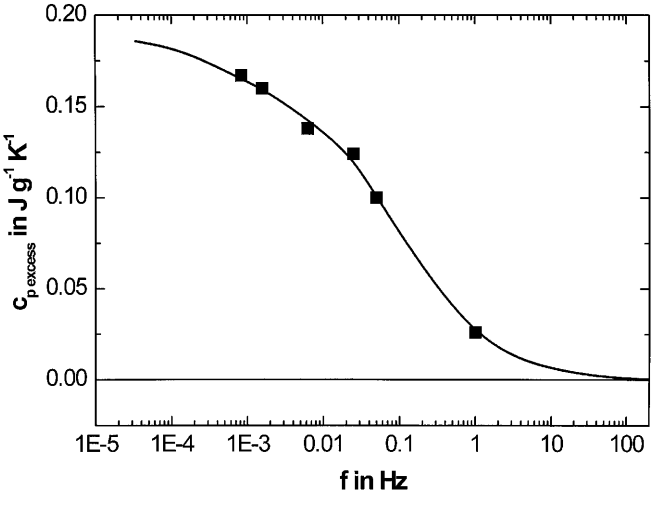

Fig. 1 Excess heat capacity of polycaprolactone after 2,000 min crystallization at 328 K as a function of modulation frequency [4]. PerkinElmer Instruments Pyris 1 DSC and alternating current calorimeter [8]

If the baseline heat capacity is available in the temperature range between the conventional glass transition and melting, it should be possible to study vitrification and devitrification of the rigid amorphous fraction (RAF) of semicrystalline polymers. There are two possible paths to reach this goal: to extend the frequency range of the heat capacity measurements to the necessary high frequencies or to study a polymer with very slow dynamics of the reversing melting so that the high-frequency limit is reached at standard frequencies of TMDSC. For PCL, as an example, frequencies above 100 Hz are necessary to measure the baseline heat capacity (Fig. 1). This is far above the TMDSC high-frequency limit of 0.1 Hz. In this work, we followed the second approach and studied bisphenol-A polycarbonate (PC) and poly(3–hydroxybutyrate) (PHB). PC was chosen for this study because of its very slow crystallization behavior [9]. Why PHB does not show reversing melting in the temperature range where it can be cold crystallized is not known. PHB is able to crystallize relatively fast and for polymers, high degrees of crystallinity (0.6–0.8) can be easily reached.

In the present work, we compare the measured baseline heat capacities of PC and PHB with estimated heat capacities due to fast molecular motions [10, 11] to detect vitrification and devitrification of the RAF.

Experimental

TMDSC, a technique described for the first time in 1971 by Gobrecht et al. [1], and the necessary data treatments are described elsewhere [1, 12–16]. If one wants to perform TMDSC measurements in a broad frequency range the results from high-sensitivity DSC apparatuses with different time constants, such as a Perkin-Elmer Pyris 1 DSC and a Setaram DSC 121, must be combined [17]. For measurements at a fixed frequency of 0.01 Hz a TA Instruments DSC 2920 was used. For the comparison of various experimental data sets, a careful temperature calibration of all instruments is necessary. The DSC instruments were calibrated at zero heating rate according to the GEFTA recommendation [18]. The calibration was checked in TMDSC mode with the smectic A to nematic transition of 8OCB [19, 20].

PCL was a commercial sample from Aldrich Chemie with a weight-average molecular weight, M_W, of 55,700 g/mol. More details about the sample are reported in Ref. [21]. PC was obtained from General Electric (trade name LEXAN) and was purified by dissolution in chloroform, filtering and precipitation in methanol [22, 23]. The weight-average molar mass and polydispersity index for PC were obtained by gel permeation chromatography in chloroform ($M_w = 28{,}400$ g/mol and $M_w/M_n = 2.04$). PHB was received from A. Mansour, University of Cairo.

The heat capacity data for these polymers in the liquid and the crystalline state, except for PHB, are available from the ATHAS data bank [11]. For PHB the heat capacity was measured for an initially amorphous sample on heating (Fig. 2). The heat capacity for liquid PHB was obtained from the line connecting the region above the glass transition (275–300 K) with the melt (450–473 K). The straight line $C_{p,\mathrm{liquid}}(T) = 1.1\ \mathrm{Jg^{-1}K^{-1}} + 0.00208\ \mathrm{Jg^{-1}K^{-2}} \times T$ is a reasonable fit for both regions and supports the linear

temperature dependence of C_p in the melt and the supercooled melt. The same linear dependence can be seen for liquid PC in Fig. 3. The heat capacity for solid PHB was obtained from a linear fit to the data below the glass transition (220–260 K). Here we assume that the heat capacity of the solid (crystalline and glassy) polymer equals the heat capacity of the glassy polymer in the temperature interval of interest. The fit yields $C_{p,\mathrm{solid}}(T) = 0.22\ \mathrm{Jg^{-1}K^{-1}} + 0.0035\ \mathrm{Jg^{-1}K^{-2}} \times T$. The same line was obtained for the semicrystalline PHB (Fig. 7) and supports the assumption of equal heat capacities for crystalline and glassy polymers close to the glass-transition temperature.

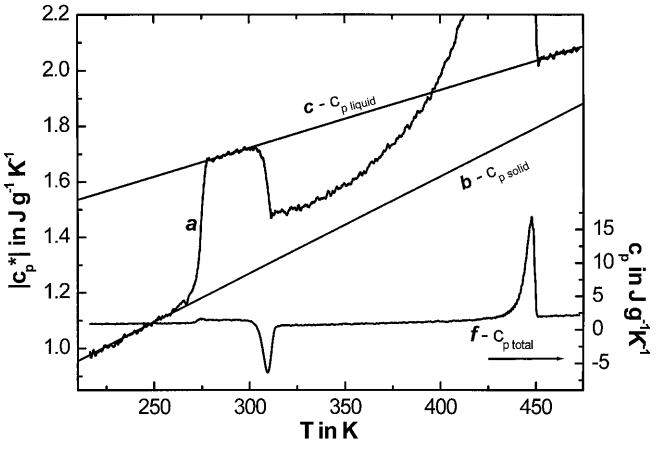

Fig. 2 Temperature-modulated differential scanning calorimetry (*TMDSC*) scan measurement of initially amorphous poly(3-hydroxybutyrate) (*PHB*) at an underlying heating rate of 1 $\mathrm{Kmin^{-1}}$, a temperature amplitude of 0.4 K and a period of 60 s, *curve a*. *Curves b* and *c* correspond to heat capacities for solid and liquid PHB, respectively, see text. *Curve f* shows the total heat capacity. PerkinElmer Instruments Pyris 1 DSC

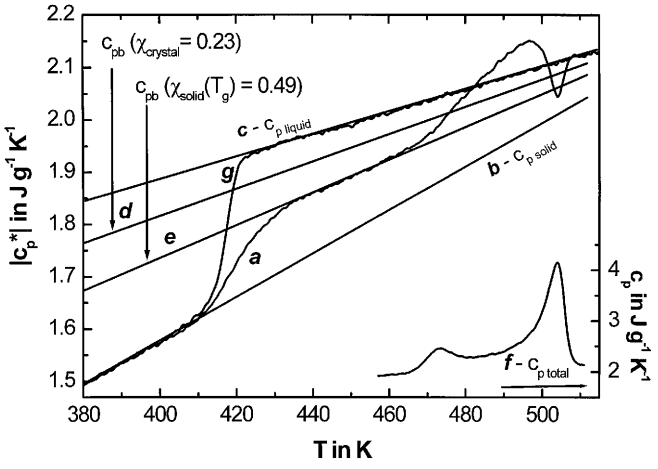

Fig. 3 TMDSC scan measurement of semicrystalline bisphenol-A polycarbonate (*PC*) at an underlying heating rate of 0.5 $\mathrm{Kmin^{-1}}$, a temperature amplitude of 0.5 K and a period of 100 s, *curve a*. *Curves b* and *c* correspond to heat capacities from the ATHAS data bank for crystalline and liquid PC, respectively. *Curve d* was estimated from a two-phase model, Eq. (1), and *curve e* from a three-phase model, Eq. (2), using $\chi_{\mathrm{solid}}(T_g)$. *Curve f* shows the total heat capacity in the melting region, while *curve g* shows the measured heat capacity for the amorphous PC. TA Instruments DSC 2920

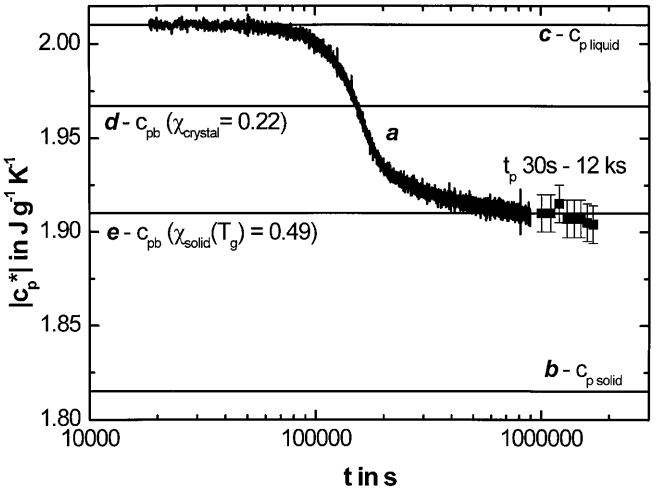

Fig. 4 Time evolution of heat capacity during quasiisothermal crystallization of PC at 456.8 K, temperature amplitude 0.5 K and period 100 s, *curve a*. *Curves b* and *c* correspond to crystalline and liquid heat capacities from the ATHAS data bank, respectively. *Curve d* was estimated from a two-phase model, Eq. (1), and *curve e* from a three-phase model, Eq. (2), using $\chi_{\mathrm{solid}}(T_g)$ from Eq. (3). The *squares* represent measurements at modulation periods ranging from 30 to 12,000 s. TA Instruments DSC 2920, PerkinElmer Instruments Pyris 1 DSC and Setaram DSC 121

Because heat capacities are additive, the baseline heat capacity can be obtained from mixing rules. In a first approximation, the expected baseline heat capacity, $C_{p,b}$, for the semicrystalline sample can be calculated using a two-phase model according to

$$C_{p,\mathrm{b}}(T,t) = \chi_{\mathrm{crystal}}(T,t)C_{p,\mathrm{crystal}}(T) + \left[1 - \chi_{\mathrm{crystal}}(T,t)\right]C_{p,\mathrm{liquid}}(T) \ , \tag{1}$$

with $C_{p,\mathrm{crystal}}$ the specific heat capacity for the crystal, which is assumed to equal to $C_{p,\mathrm{solid}}$, $C_{p,\mathrm{liquid}}$ the specific heat capacity for the melt and χ_{crystal} the degree of crystallinity. For most polymers, deviations from such a simple two-phase model are observed [24, 25]. By introducing a RAF the baseline heat capacity can be obtained from

$$C_{p,\mathrm{b}}(T,t) = \chi_{\mathrm{solid}}(T,t)C_{p,\mathrm{solid}}(T) + [1 - \chi_{\mathrm{solid}}(T,t)]C_{p,\mathrm{liquid}}(T) \ , \tag{2}$$

with $C_{p,\mathrm{solid}}$ the specific heat capacity of the solid fraction, $\chi_{\mathrm{solid}}(T, t)$. The solid fraction contains the crystalline and the RAF. For most polymers, $C_{p,\mathrm{solid}}$ equals $C_{p,\mathrm{crystal}}$ and is available from Ref. [11]. At the glass-transition temperature $\chi_{\mathrm{solid}}(T_g)$ can be obtained from the heat capacity increment at T_g.

$$\chi_{\mathrm{solid}}(T_g) = 1 - \Delta C_p/\Delta C_{p,\mathrm{amorph}} \ , \tag{3}$$

where ΔC_p is the heat capacity increment of the semicrystalline sample, while $\Delta C_{p,\mathrm{amorph}}$ is that of the totally amorphous sample. In order to obtain $\chi_{\mathrm{solid}}(T_g)$ of the isothermally crystallized polymers the samples were cooled below T_g after crystallization and ΔC_p was obtained from a TMDSC scan measurement on heating above the melting temperature. The heat of fusion was determined from $C_{p,\mathrm{total}}$ from this scan and $\chi_{\mathrm{crystal}}(T)$ was calculated according to the procedure suggested by Mathot [26]. Knowing the solid and the crystalline fraction the RAF can be estimated from

$$\mathrm{RAF} = \chi_{\mathrm{solid}}(T,t) - \chi_{\mathrm{crystal}}(T,t) \ . \tag{4}$$

Results

The modulus of the complex heat capacity and the total heat capacity from a TMDSC heating scan of semicrystalline PC and PHB are shown in Figs. 3 and 7, respectively.

The measured heat capacity for the amorphous PC, curve g, equals the expected line from the ATHAS data bank for the liquid above T_g and that for the crystal below T_g. No difference between the heat capacity of the semicrystalline and the glassy amorphous PC can be observed below T_g. This supports the assumption of equal heat capacities for crystalline and glassy polymers close to T_g. The measured heat capacity from the semicrystalline PC above T_g is significantly smaller than the baseline heat capacity estimated from a two-phase model, curve d, indicating a significant RAF. Curve e in Fig. 3 was estimated from a three-phase model, Eq. (2). The solid fraction, $\chi_{solid}(T_g)$, was determined at the glass transition from Eq. (3). In the temperature interval above the glass transition and below 460 K, no deviations of the measured heat capacity from the baseline heat capacity, curve e, can be observed. In contrast to most other semicrystalline polymers there is, on the time scale of the measurement ($t_p = 100$ s), no reversing melting and no excess heat capacity in this temperature interval. Because the maximum crystallization rate of PC is observed at around 460 K there is a chance to study the crystallization of PC at 460 K without the occurrence of an excess heat capacity at 0.01 Hz.

The time evolution of the heat capacity during isothermal crystallization of PC at 456.8 K and PHB at 296 K is shown in Figs. 4 and 5, respectively. To check whether or not the baseline heat capacity was measured, the frequency dependence was studied at the end of the crystallization (points). No frequency depen-

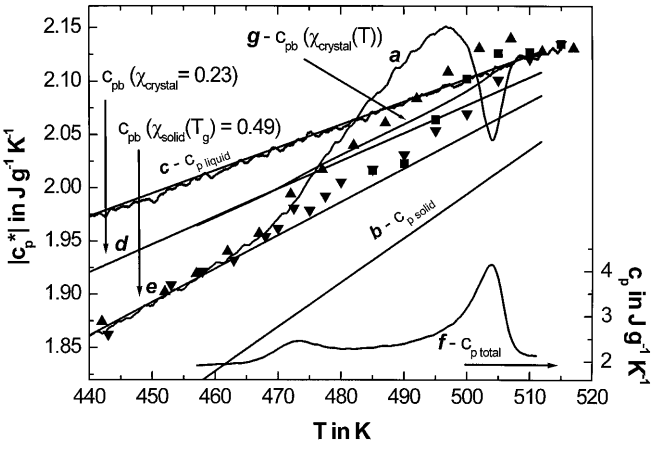

Fig. 6 Melting region of PC, magnified part of Fig. 3. Curves as in Fig. 3 except *curve g*, which now represents the baseline heat capacity from a two-phase model, Eq. (1), taking into account the changes in crystallinity in the main melting region. The *points* show the heat capacities from quasiisothermal TMDSC measurements on stepwise increasing temperatures. The data from independent measurements were taken after 15 min (π) at $t_p = 100$ s and after 10 h at $t_p = 100$ s (θ) and at $t_p = 1000$ s (■)

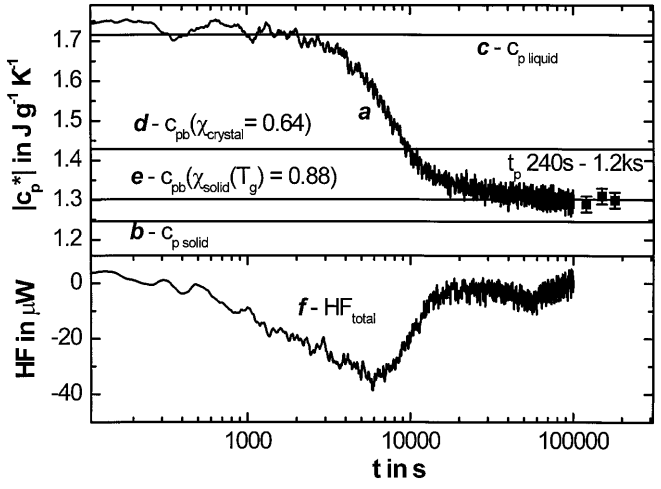

Fig. 5 Time evolution of heat capacity during quasiisothermal crystallization of PHB at 296 K, temperature amplitude 0.5 K and period 100 s, *curve a*. *Curves b* and *c* correspond to solid and liquid heat capacities, respectively. *Curve d* was estimated from a two-phase model, Eq. (1) and *curve e* from a three-phase model, Eq. (2), using $\chi_{solid}(T_g)$ from Eq. (3). The *squares* represent measurements at modulation periods ranging from 240 to 1,200 s. *Curve f* shows the exothermal effect in the total heat flow. PerkinElmer Instruments Pyris1 DSC

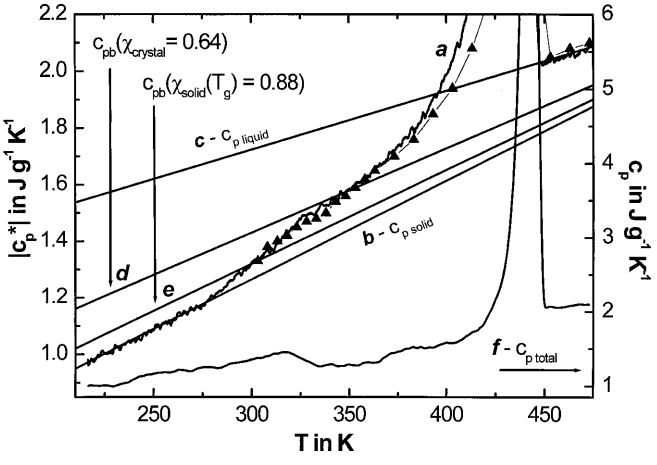

Fig. 7 TMDSC scan (*lines*) measurements of semicrystalline PHB at an underlying heating rate of 1 Kmin^{-1}, a temperature amplitude of 0.4 K and a period of 60 s, *curve a*. *Curves b* and *c* correspond to heat capacities for solid and liquid PHB, respectively. *Curve d* was estimated from a two-phase model, Eq. (1), and *curve e* from a three-phase model, Eq. (2), using data from T_g. The *triangles* show the heat capacities from quasiisothermal TMDSC measurements on stepwise increasing temperatures. The data were taken after 30 min. *Curve f* shows the total heat capacity. PerkinElmer Instruments Pyris 1 DSC

dence of the measured heat capacity can be seen, indicating the absence of reversing melting and that the baseline heat capacity was obtained. The measured heat capacity becomes smaller than the baseline heat capacity according to Eq. (1), curve d, indicating the occurrence of a significant RAF during the crystallization process. On the other hand, the expected heat capacity, taking into account the RAF obtained at the glass transition, line e, is in perfect agreement with the measured value at the end of isothermal crystallization. There is no difference in the amount of the RAF at crystallization and at the glass-transition temperature; also T_g is more than 30 K below the crystallization temperature in the case of PC. Therefore, we can conclude that the total RAF of PC and PHB is established (vitrified) during the isothermal crystallization. No additional vitrification occurs on cooling from the crystallization to the glass-transition temperature.

Next, the question arises at what temperature the RAF devitrifies on heating? Is devitrification smeared over a broad temperature interval? Does it occur before the crystals melt? Or is devitrification of the RAF part of the main melting? To answer these questions the heat capacity was measured on heating and was compared with expected baseline heat capacities (see Figs. 6, 7 for PC and PHB, respectively).

The heat capacity measured at scanning through the melting region of PC, Figs. 3 and 6 curve a, shows deviations from the baseline heat capacity in the temperature range 460–510 K probably owing to reorganization on slow heating (0.5 $Kmin^{-1}$). To measure the heat capacity without contributions from reorganization, quasiisothermal TMDSC measurements at stepwise increasing temperatures were performed. The results in the temperature range above the glass transition (Fig. 3) are shown in Fig. 6.

At the lowest endotherm, between 460 and 485 K, a steplike increase in the heat capacity can be observed. The heat capacity starts to deviate from the baseline heat capacity obtained from a three-phase model including RAF, Eq. (2) curve e, and around 480 K it is close to the baseline heat capacity obtained from a two-phase model, Eq. (1) curves d and g. In Eq. (1), only crystalline and liquid (mobile amorphous) material is taken into account. This increase in heat capacity cannot be explained by the decrease in crystallinity due to the lowest melting endotherm between 465 and 485 K. The expected increase due to the lowest endotherm can be seen as the difference between curve g, which was calculated, from Eq. (1) assuming temperature-dependent crystallinity, and curve d, which was calculated assuming constant crystallinity.

At higher temperatures, below the main melting, the heat capacity becomes a little larger than the increasing baseline heat capacity as estimated from the temperature-dependent crystallinity and Eq. (1), curve g, because of some excess heat capacity. The heat capacity decreases during the isothermal measurement. After 10 h the value is again close to the baseline heat capacity obtained from a three-phase model, Eq. (2). Up to 490 K no frequency dependence can be observed in the frequency range 0.01–0.001 Hz. Above 490 K, in the main melting peak, also for the quasiisothermal measurements on a time scale of 100 s, an excess heat capacity (reversing melting) as well as a frequency dependence can be observed (Fig. 6).

Basically the same behavior as for PC can be seen for PHB on heating (Fig. 7). Again, at the lowest endotherm, around 320 K, a second step in the heat capacity towards the expected value from the two-phase model can be observed. Because PHB crystallizes fast, the isothermal crystallization was performed close to the glass transition to be able to follow the crystallization process. Consequently, premelting is not well separated from the glass transition in temperature.

Discussion

For PC and PHB a significant RAF can be determined from the step of the heat capacity at the glass transition. By taking into account the crystalline, the rigid amorphous and the mobile amorphous fractions, information about the phases of different molecular mobility can be obtained. For PC after 11 days crystallization at 456.8 K the crystallinity was 0.23, the RAF 0.26 and the mobile amorphous fraction 0.51. For PHB after crystallization at 296 K for 28 h, the values were 0.64, 0.22 and 0.12, respectively. From the TMDSC scan measurements no excess heat capacity can be detected for either of the semicrystalline polymers at temperatures above the glass transition and below the lowest endotherm. While PC crystallizes extremely slowly, PHB crystallizes reasonably fast, like poly(ethylene terephthalate) (PET), poly(ether ether ketone) and poly(ethylene naphthalate), and high degrees of crystallinity can be realized. We do not know why these two polymers show no excess heat capacity at periods of about 100 s, indicating the absence of reversing melting, while other polymers show large excess heat capacities [27–30].

The absence of excess heat capacities in a temperature range suitable for crystallization experiments allows us to study the baseline heat capacity as a function of time and to compare the measured one with expected values (Figs. 4 and 5). For PC and PHB the measured heat capacity becomes significantly smaller than the baseline heat capacity expected from a two-phase model, Eq. (1). It clearly demonstrates that for these polymers a significant portion of the RAF is formed during the isothermal crystallization process. Furthermore, a perfect match between the measured heat capacity at the end of crystallization and the expected baseline heat

capacity from Eq. (2) can be seen. Because line e was obtained, for both polymers, from Eq. (2) using the RAF determined from the heat capacity increment at T_g, there are no indications for changes in the amount of the RAF on cooling from the crystallization temperature to the glass transition. In other words, the whole RAF, detected at T_g, was established during the quasiisothermal crystallization. From these observations we can conclude that, at least for PC and PHB, there is no broad glass transition of the RAF somewhere between the crystallization temperature and T_g. Consequently, vitrification of the RAF results from the crystallization process itself. Vitrification of the RAF is the result of morphological changes and is not due to cooling below a sometimes assumed second glass-transition temperature in semicrystalline polymers.

Because there is no generally accepted theory for polymer crystallization, we discuss these findings in the light of Marand's description of PC crystallization [22] and Strobl's view on polymer crystallization [31].

Marrand and coworkers describe the crystallization of PC as a two-step process. First lamellae are formed which build up lamella stacks and finally spherulites. After completion of this step, small crystals are formed between the existing lamellae. The second step, the formation of small crystals with a large specific surface, seems to be the crucial step with respect to the formation of the RAF. A prerequisite for the formation of these small crystals is some mobility of the melt surrounding the growing crystals. If the RAF is assumed to be a consequence of the formation of the primary lamellae, there would be no chance to form new crystals because the material is vitrified. Following this model, the consequence is that the RAF results from the vitrification of the amorphous material in the neighborhood of the small secondary crystals. The reason for the vitrification is primarily the increase in constraints for the amorphous material on a molecular level and/or a decrease in the volume of the remaining amorphous domains below the necessary volume to establish a cooperatively rearranging region (confinement effects) [32]. Consequently, the vitrification of the RAF stops further crystallization because vitrification of the amorphous material around the growing crystals prevents all large scale molecular motions which are necessary for the attachment of chain segments to the growth face.

On heating, the constraints should disappear as soon as the small crystals melt. According to Marand this happens at the lowest endotherm [9, 22, 23, 33]. From Figs. 6 and 7 it can be seen that just in the temperature range of the lowest endotherm the heat capacity initially shows a steplike increase and becomes very close to the value expected from a two-phase model, Eq. (1). Consequently, also on heating there is no common temperature-induced separate glass transition of the RAF. The devitrification of the RAF is, as vitrification, a direct consequence of morphological and not temperature changes.

Strobl's model for the formation of crystal lamellae assumes a three-step process [31]. In the first step, a layer with mesomorphic structure arises. This phase consists of incompletely stretched and refolded chains and corresponds in its thermodynamic properties rather to the isotropic melt than to the crystal. These layers should have a minimal thickness to be stable in the melt. The attachment of further partly stretched segments of appropriate length is assumed to result in the lateral growth. Owing to the still high flexibility of the chains, cooperative rearrangements yield a thickening and perfection of the layers. The gaining of a critical thickness results in the rigidity of the layer and stops the thickening. In the second step of the model, granular crystalline layers (blocks) arise. This transition should appear spontaneously, with no need for nucleation, and is thought to be of second order. The third step characterizes the merging of the blocks to homogeneous crystal lamellae with the thickness of the original blocks. For the first two steps the growing structures are assumed to be in dynamic equilibrium with the surrounding melt and fluctuations of the structure may appear. Only the last step, the merging of the blocks, yields a more stable structure that melts at higher temperatures. We relate our observations to the second and third steps. In the case that the surroundings of the granular lamellae are vitrified owing to the thickening of the lamellae, the vitrified material will prevent the blocks from merging because of a lack of mobility. Finally, the lack of mobility keeps the granular structures and they will melt at temperatures close to the crystallization temperature. As in Marand's model, the melting of these structures will release the constraints for the amorphous material and it devitrifies. It is assumed that this process occurs at the lowest endotherm.

In both models, devitrification of the RAF in conjunction with melting of a small fraction of the crystalline material results in the possibility of large-scale molecular motions which yield the formation of new crystals. The growth of these newly formed crystals will again result in the vitrification of their surroundings and finally prevent further crystallization. The quasiisothermal measurements for 10 h support this view (Fig. 6). Only after devitrification of the RAF, step in heat capacity around 470 K in the measurements after 15 min, can significant reorganization (decreasing heat capacity) be observed. After 10 h the heat capacity reaches values which are close to that expected from Eq. (2), taking into account the RAF. Only near the main melting peak is the annealing time not long enough to reach a steady state and, consequently, also after 10 h a significant excess heat capacity, showing frequency dependence, can be observed. This is in agreement with the observations of Lu and Cebe [34] for poly(phenylene

sulfide) but does not support the view of Song and Hourston [35] considering a broad glass transition of the RAF for PET.

Conclusion

For PC and PHB the asymptotic value of the heat capacity at high frequencies (Fig. 1) can be measured by TMDSC. This allows the measurement of the baseline heat capacity and the study of the the formation of the RAF. For PC and PHB, the RAF is established during isothermal crystallization as can be seen from Figs. 4 and 5. Devitrification of the RAF seems to be related to the lowest endotherm (Figs. 6, 7). The immobilization of the amorphous material around less perfect crystals, which are formed during isothermal crystallization, results in the vitrification of the RAF during crystallization and in its devitrification during melting. Our results can be explained by Marand's [22] and Strobl's [31] models of polymer crystallization. From our data it is not possible to favor one of these models; however, our results illustrate the interplay between the molecular mobility of the melt and the polymer crystallization. Hopefully, a more complex view, taking into account the structure and the properties of the melt surrounding the growing crystals, will help to solve some of the still open questions of polymer crystallization [36]. The frequency-dependent heat capacity, in the high-frequency limit, yields quantitative information about fractions of different mobility during the crystallization process and how the mobility of the melt is influenced by the crystallization process itself. From the step in the heat capacity versus frequency, information about the characteristic timescale of the attachment and detachment processes of polymer segments at the crystal surface can be obtained. In order to perform such measurements, the frequency range of the heat capacity measurements has to be enlarged.

Acknowledgements We are thankful to H. Marand, Blacksburg, Va., for supplying the PC sample and to A. Mansour, Cairo, for supplying the PHB sample and to both for stimulating discussions. This research was supported by the European Commission (grant IC15CT96–0821), the German Science Foundation (grant DFG Schi-331/5–1) (A.W.) and the Government of Egypt (A.M.). We acknowledge support by PerkinElmer Instruments and TA Instruments.

References

1. Gobrecht H, Hamann K, Willers G (1971) J Phys E Sci Instrum 4:21
2. Birge NO, Nagel SR (1985) Phys Rev Lett 54:2674
3. Weyer S, Hensel A, Schick C (1997) Thermochim Acta 304/305:251
4. Schick C, Merzlyakov M, Minakov A, Wurm A (2000) J Therm Anal Cal 59:279
5. Saruyama Y (1999) Thermochim Acta 330:101
6. Okazaki I, Wunderlich B (1997) Macromol 30:1758
7. Hu W, Albrecht T, Strobl G (1999) Macromol 32:7548
8. Minakov AA, Bugoslavsky Yu, Schick C (1998) Thermochim Acta 317:117
9. Sohn S (2000) PhD thesis. Virginia Polytechnic and State University
10. Wunderlich B, Pyda MJ (1999) Reinf Plast Compos 18:487
11. (a) Wunderlich B (1995) Pure Appl Chem 67:1019; (b) http://web.utk.edu/~athas/databank/intro.html
12. Wunderlich B, Jin YM, Boller A (1994) Thermochim Acta 238:277
13. Reading M (1993) Trends Polym Sci 8:248
14. Schawe JEK (1995) Thermochim Acta 260:1
15. (a) Merzlyakov M, Schick C (1999) Thermochim Acta 330:55; (b) Merzlyakov M, Schick C (1999) Thermochim Acta 330:65
16. Weyer S, Hensel A, Schick C (1997) Thermochim Acta 304/305:267
17. Merzlyakov M, Wurm A, Zorzut M, Schick C (1999) J Macromol Sci Phys 38:1045
18. Sarge SM, Hemminger W, Gmelin E, Höhne GWH, Cammenga HK, Eysel W (1997) J Therm Anal 49:1125
19. Hensel A, Schick C (1997) Thermochim Acta 304/305:229
20. Schick C, Jonsson U, Vassiliev T, Minakov A, Schawe J, Scherrenberg R, Lörinczy D (2000) Thermochim Acta 347:53
21. Skoglund P, Fransson A (1996) J Appl Polym Sci 61:2455
22. Sohn S, Alizadeh A, Marand H (2000) Polymer 41:8879
23. Alizadeh A, Sohn S, Quinn J, Marand H, Shank L, Iler HD (submitted May 2000) Macromolecules
24. Ishida Y, Yamafuji K, Ito H, Takayanagi M (1962) Kolloid Z Z Polym 184:97
25. Suzuki H, Grebowicz J, Wunderlich B (1985) Makromol Chem 186:1109
26. Mathot VBF (1994) Calorimetry and thermal analysis. Hanser, Munich, p 120
27. Wurm A, Merzlykov M, Schick C (1999) J Macromol Sci Phys 38:693
28. Toda A, Tomita C, Hikosaka M, Saruyama Y (1997) Polymer 38:2849
29. Wurm A, Merzlykov M, Schick C (1998) Colloid Polym Sci 276:289
30. Scherrenberg R, Mathot VBF, Van Hemmelrijck A (1999) Thermochim Acta 330:3
31. Strobl G (2000) Eur Phys J E 3:165
32. Donth E (1993) Relaxation and thermodynamics in polymers. Akademie, Berlin, p 131
33. Marand H, Alizadeh A, Farmer R, Desai R, Velikov V (2000) Macromolecules 33:3392
34. Lu SX, Cebe P (1996) Polymer 37:4857
35. Song M, Hourston DJ (1998) J Therm Anal Cal 54:651
36. Geil PH (2000) Polymer 41:8983